

Discontinuous tracks in arsenic-doped crystalline $\text{Si}_{0.5}\text{Ge}_{0.5}$ alloy layers

P. I. Gaiduk,^{1,*} A. Nylandsted Larsen,¹ C. Trautmann,² and M. Toulemonde³

¹*Institute of Physics and Astronomy, University of Aarhus, Ny Munkegade, DK-8000, Aarhus C. Denmark*

²*Gesellschaft für Schwerionenforschung (GSI), Planckstrasse 1, D-64291 Darmstadt, Germany*

³*Centre Interdisciplinaire de Recherches avec les Ions Lourds BP 5133, F 14070-Caen-Cedex 5, France*

(Received 27 December 2001; published 22 July 2002)

We report the observation of tracks in single-crystalline $\text{Si}_{0.5}\text{Ge}_{0.5}$ alloy layers irradiated with 1.3-GeV U ions in the electronic stopping-power regime. Transmission electron microscopy in both conventional and high-resolution mode reveals more or less discontinuous tracks depending on the composition of the $\text{Si}_{1-x}\text{Ge}_x$ alloy and on the arsenic doping level. The morphology and the atomic structure of the tracks are analyzed. The results are discussed in the frame of the thermal-spike approach which assumes both track melting and imperfect crystallization.

DOI: 10.1103/PhysRevB.66.045316

PACS number(s): 81.07.-b, 61.80.Jh, 61.46.+w, 61.72.Qq

I. INTRODUCTION

When penetrating solids, swift heavy ions in the energy range of several hundreds of MeV–GeV slow down due to electronic stopping (S_e) which prevail over the nuclear stopping (S_n) by a factor of about 10^3 .^{1,2} Above a material-dependent S_e threshold, the high density of electronic excitations and ionizations may produce so-called latent tracks.² They are long and narrow cylindrical defect zones of modified structure surrounded by the undisturbed host matrix. Tracks formed in polymers or other dielectrics can be used for the fabrication of nanoporous filters. In many other materials, such as semiconductors, metals and alloys, or high- T_c superconductors the electrical and/or mechanical properties can be modified.²

While tracks are routinely formed in numerous dielectrics, in some selected metals and amorphous semiconductors,^{2,3} the situation is more complex in single-crystalline semiconductors. Clear evidence of track formation is reported for some compound semiconductors, e.g., GeS^4 and InP^{5-8} . However, no tracks were found in single-crystalline GaAs and GaP.^{8,9} No clear correlation of track formation with the main characteristics of semiconductors (band gap E_g , melting point T_m , electrical properties) exists. For example, under identical irradiation conditions, tracks are created in InP ($E_g=1.34$ eV, $T_m=1060$ °C), but no tracks are found in semi-insulating GaAs ($E_g=1.44$ eV, $T_m=1240$ °C).⁸ To our knowledge, there is no evidence that *monoatomic* swift heavy ions produce tracks in single-crystalline Si ($E_g=1.12$ eV, $T_m=1412$ °C), Ge ($E_g=0.66$ eV, $T_m=937$ °C), GaP ($E_g=2.26$ eV, $T_m=1457$ °C), or diamond ($E_g=5.46-5.6$ eV, $T_m=4373$ °C).^{9,10-12} In the case of single-crystalline Si and Ge, this has been tested for different ion species (oxygen to uranium) in the MeV–GeV energy range corresponding to energy losses up to 28 keV/nm (Si) and 38 keV/nm (Ge). The only defects, observed by deep level transient spectroscopy (DLTS),^{11,12} are similar to those obtained under the irradiation with electrons or protons,¹³ namely *A* centers (vacancy-oxygen complex), *E* centers (vacancy-doping impurity complex), and divacancies. It has also been observed that the irradiation of single-crystalline Si with, e.g., 340-MeV Xe ions results in efficient annealing of

defects previously introduced by protons.¹⁴ Similar annealing or “electronic energy-loss-induced self-recrystallization” has been reported for Ge^{9,10} and Si, C (diamond), and GaP.⁹

The situation is different when irradiating single-crystalline Si (Ref. 15) and Ge (Ref. 16) with accelerated cluster projectiles because the stopping powers (up to 57 keV/nm) are even larger than in the case of uranium ions. On a length of typically 100 nm, 20–40-MeV C_{60} fullerenes produce amorphous tracks with a diameter of about 10 nm. Under the electron beam of the transmission electron microscope (TEM), these tracks are rather unstable and recrystallize rapidly.¹⁵ However, for an adequate interpretation of these results several aspects, such as the contribution of nuclear stopping and the small path length before the clusters components become decorrelated,^{15,16} have to be taken into account. In addition, a direct comparison of C_{60} projectiles and monoatomic ions is not straightforward because the relatively low cluster velocity leads to a short range of the δ electrons and therefore the energy is deposited into a smaller volume.

In the present study, the formation of tracks was investigated in a single-crystalline $\text{Si}_{0.5}\text{Ge}_{0.5}$ alloy, epitaxially grown on a (001) Si substrate and doped with arsenic. Using 1.3-GeV U projectiles ($S_e=33.8$ keV/nm), we have found evidence for discontinuous tracks in a group-IV semiconductor. The experiments were motivated by the prediction⁵⁻⁸ that track formation in crystalline semiconductors requires at least two main criteria, namely local melting along the ion trajectory and *imperfect* recrystallization. The latter is possible if the solidification starts from a liquid-solid interface containing a large number of defects⁵⁻⁸ or *distorted bonds*. For the verification of this idea a $\text{Si}_{1-x}\text{Ge}_x$ alloy seems to be a good candidate because, (i) the two atom species are different in mass and size, (ii) Si and Ge are fully miscible and form random substitutional alloys at all compositions, and (iii) $\text{Si}_{1-x}\text{Ge}_x$ alloys can be epitaxially grown exhibiting excellent crystalline quality both in strained and strain-relaxed modes.¹⁷

II. EXPERIMENTAL PROCEDURE

For our experiments, strain-relaxed, epitaxial *p*-type $\text{Si}_{0.5}\text{Ge}_{0.5}$ layers were grown by molecular-beam epitaxy

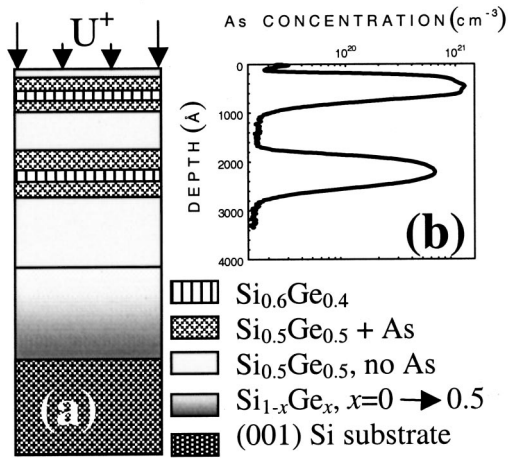


FIG. 1. (a) Sketch of the MBE-grown sample used in this study. (b) As depth distribution profile in the sample measured by SIMS.

(MBE) on (001) silicon wafers using the stepwise compositionally grading technique.¹⁸ First, a silicon buffer layer 0.1 μm thick was grown, followed by a compositionally graded buffer layer of an average grading of about 30% Ge/ μm . On top of this, a uniform layer of $\text{Si}_{0.5}\text{Ge}_{0.5}$ was grown at a temperature of 800 $^{\circ}\text{C}$ to a total thickness of 1.3 μm [Fig. 1(a)]. Finally, a highly doped 0.3- μm -thick surface layer was grown at 450 $^{\circ}\text{C}$ by *in situ* 1-keV As ion implantation at two different depth intervals (20–80 and 180–280 nm). They are partly covered with two 5-nm $\text{Si}_{0.6}\text{Ge}_{0.4}$ spikes as shown in Fig. 1(a). From the secondary-ion mass spectrometry (SIMS) depth profile [Fig. 1(b)], the As peak concentration in the layer is about $1.1 \times 10^{21} \text{ cm}^{-2}$, which exceeds the solid solubility limit of As in a $\text{Si}_{0.5}\text{Ge}_{0.5}$ alloy by about a factor of 10.¹⁹ However, the crystalline quality of the layers remains excellent as evidenced by transmission electron microscopy (TEM). For reasons which also will be discussed below, arsenic was selected as dopant due to its strong tendency to precipitate in the $\text{Si}_{1-x}\text{Ge}_x$ alloy layers into GeAs nanocrystals, as found after rapid thermal annealing.¹⁹

The wafers were irradiated at room temperature with 1.3-GeV U^{238} ions to a fluence of 10^{10} cm^{-2} at a constant flux around $2 \times 10^8 \text{ cm}^{-2} \text{ s}^{-1}$. According to TRIM95 calculations,²⁰ the electronic and nuclear stopping powers are $S_e = 33.8 \text{ keV/nm}$ and $S_n = 0.024 \text{ keV/nm}$, respectively. The structure of the samples was investigated by TEM using a Philips CM20 (200-keV) microscope. The TEM samples were prepared in both plan-view (PV) and cross-section (X) geometries using a routine procedure consisting of successive mechanical polishing and ion-beam milling at room temperature.

III. EXPERIMENTAL RESULTS

Figure 2 shows a representative bright-field (BF) PV image of a sample inclined in the microscope with respect to the electron beam. Dotlike and elongated dark spots of an average size of about 3–10 nm are aligned along the projectile trajectories like a string of pearls running parallel to each other. Due to the discontinuous nature of the track, the defect

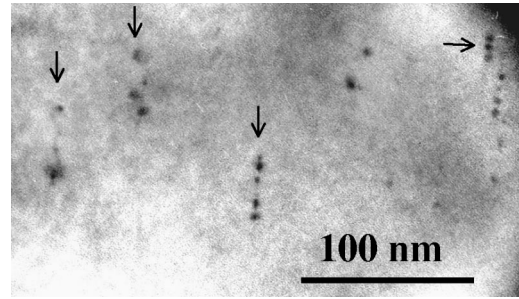


FIG. 2. Bright-field PVTEM image of the structure of the $\text{Si}_{0.5}\text{Ge}_{0.5}$ alloy layer irradiated with swift U ions at room temperature. The arrows indicate the tracks. To demonstrate a possible depth correlation of the defects, the sample was inclined with respect to the electron beam.

structure and the diameters strongly vary along the ion trajectory. Tracks typically consist of two to five separated dots. Some tracks are considerably longer containing even a few tens of dots. However, there are also individual single dots without any close neighboring dots. The density of the isolated dots together with the discontinuous tracks (consisting of three or more dots) is estimated to be around $(8-9) \times 10^9 \text{ cm}^{-2}$ in good agreement with the applied ion fluence. In contrast, the total number of extended tracks amounts only to about $(1-3) \times 10^9 \text{ cm}^{-2}$, i.e., 10–30% of all defects.

In most conditions of the BF imaging, the defects are practically invisible or have a very weak contrast. The maximum image contrast of the defects is obtained for two-beam diffraction conditions with a large deviation parameter $s \gg 0$. This behavior indicates that the core region of the track has a *crystalline structure*. Clear evidence is given by the high-resolution TEM image (PV) in Fig. 3 presenting a cross section of a single track in a $\text{Si}_{0.5}\text{Ge}_{0.5}$ alloy layer. The inner track zone (dark) has a diameter of 4–5 nm and exhibits strong image contrast of the atomic chains. This gives clear evidence of the good crystalline quality of the core region. The periphery (light) is 10 nm in diameter and shows a rather smooth contrast most likely due to a large number of point defects and defect clusters. The boundary between the core

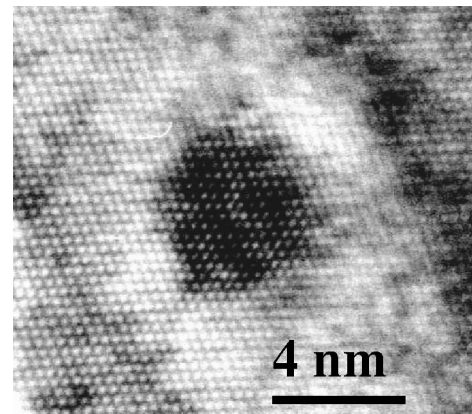


FIG. 3. High-resolution (HR) TEM image of a 1.3-GeV U irradiated $\text{Si}_{0.5}\text{Ge}_{0.5}$ alloy layer showing the typical atomic structure of the track. The image was obtained in plan-view geometry.

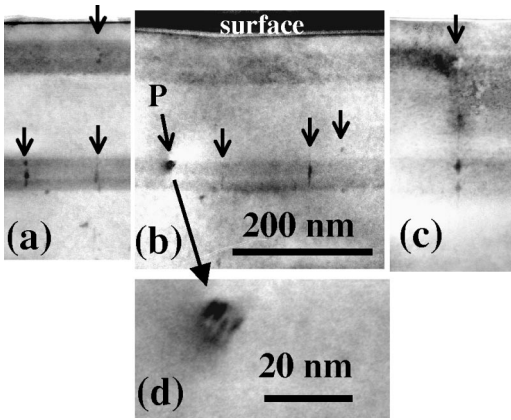


FIG. 4. Bright-field XTEM images of the structure of the $\text{Si}_{0.5}\text{Ge}_{0.5}$ alloy layer irradiated with swift U ions taken from different regions of the sample. The small arrows indicate the tracks, (P) shows GeAs precipitate, (d) shows enlarged image of a 11.5-nm GeAs precipitate.

and the periphery of the track is rather sharp and (111) faceted while it is diffuse between the periphery and the matrix.

We also imaged the cross section of different regions of the samples by BF XTEM (Fig. 4). No tracks could be discovered in the Si substrate, whereas in the entire $\text{Si}_{0.5}\text{Ge}_{0.5}$ layer, U ions created more or less homogeneously distributed individual dotlike defects. When the trajectories of the projectiles pass through the two As-doped bands of $\text{Si}_{0.5}\text{Ge}_{0.5}$ [the corresponding track segments are indicated by arrows in Figs. 4(a)–(c)], the probability of defect formation increases significantly and tracks of discontinuous character are created. In this layer there is a clear tendency of separated spots to transform into continuous or elongated track segments. In addition to the tracks, some areas show larger circular defects [indicated as “P” in Fig. 4(b)] in the As-doped layers. They have a spherical shape with a diameter of about 10 nm. In two-beam diffraction conditions, they exhibit a sharp black-white contrast. In micrographs taken far away from any diffraction vector, the deformation contrast disappears and the defects are seen as circular or slightly faceted spots with a dark uniform contrast. Such a behavior indicates that the defects are inclusions involving atoms of higher masses than in the surrounding matrix. Unfortunately, the number density and the size of the defects is too small to perform electron diffraction and/or x-ray microanalysis. However, in accordance with more recent investigations,¹⁹ these defects can be ascribed to GeAs precipitates. Additional support for this assumption is given by the Moiré-fringe contrast resolved, e.g., in Fig. 4(d) with a fringe spacing similar to that in Ref. 19.

IV. DISCUSSION

Summarizing our experimental observation, clear evidence is found that GeV U ions induce track formation in semiconducting $\text{Si}_{0.5}\text{Ge}_{0.5}$ layers. This is in contrast to the inhibited track formation in pure Si and Ge.^{9,11,12} If the thermal spike and the melting mechanism dominates the track formation process, then the melting temperature should be

one of the most critical parameters. For a $\text{Si}_{1-x}\text{Ge}_x$ alloy, the melting temperature increases *monotonically* from 938 °C (Ge) to 1412 °C (Si). Thus as a consequence we should expect track formation in pure Ge or in Ge rich alloys. Another discrepancy concerns the thermal resistivity of $\text{Si}_{1-x}\text{Ge}_x$. According to Refs. 17 and 21, the thermal resistivity of $\text{Si}_{1-x}\text{Ge}_x$ alloys at room temperature reaches a maximum in the compositional range of $x=0.2$ – 0.4 . Layers of such a composition are located in the buffer layer of our sample but contain only few dots. Finally, there is also an important argument in favor of the thermal spike mechanism given by the (111) faceted structure of the track core (Fig. 3): Assuming that the thermal spike is followed by quenching of a liquid phase,^{1–3} we have to consider recrystallization processes. It is well known for Si and Ge that the solid-phase epitaxial growth rate strongly depends on the crystallographic orientation being fast for the (100) and slow for the (111) orientation.²² A very similar observation is also reported for ultrafast melting by laser pulses where the liquid-phase growth velocity of ν is larger than 10 m/s.^{23–27} In this case the ratio of the growth velocities is found to be about $\nu_{100}/\nu_{111}=1.65$.²⁴ Different values of ν_{100} and ν_{111} are related to two individual interface morphologies and solidification mechanisms, one within 15° of the [111] orientation and a second for the remaining orientations.^{25,26} In the first case, the morphology of the liquid-solid interface is atomically smooth and the melt solidifies via two-dimensional nucleation followed by ledge motion.^{25,27} This results in an undercooling of the melt of about 35 K.²⁶ For interfaces more than 15° from the [111] orientation, the undercooling value is about 22 K and the interface is atomically rough.^{25,26} There is strong evidence in this case that the solidification of a laser-induced melt occurs via lateral passage of {111} planes.²⁷ Thus the solidification of the melt inside the track starts with a nearly circular interface and gradually transforms to a (111) faceted shape with simultaneously decreasing solidification rate. At the beginning of the recrystallization process, atomically rough interfaces and the high solidification rate produce a large number of point defects and defect clusters preferably at the periphery of the track. When the regrowth slows down, the (111) interface is finally reconstructed and the steady-state regime of solidification leads to a nearly defect-free epitaxial growth.

We therefore suggest that the quality of the crystal lattice reconstructed during the melt solidification is a critical parameter for track formation in crystalline semiconductors. In the case of a defect-free single-crystalline Si or Ge matrix, molten tracks are surrounded by a perfect crystal and epitaxial recrystallization can occur during quenching of the thermal spike. Undistorted covalent bonds fixed at the tetrahedral angles ensure good quality of the epitaxial regrowth of the track. However, at high regrowth velocities, the reconstructed crystal is obviously not perfect but includes a number of defects as, e.g., registered by DLTS.^{11,12} The situation is different if the crystal matrix contains already a large number of defects; then the recrystallization at the track interface may be hindered and the liquid is quenched as amorphous phase (see, e.g., Refs. 5–8). A crystalline matrix consisting of atoms of very different masses, size, and type or length of

the atomic bonds can also be considered as strongly defected because the foreign atoms change the atomic order in the host matrix. In this case, the quality of the reconstructed lattice will be affected by differences in the atomic structure of the melt and solid phase, which may depend on the composition of the given alloy. In $\text{Si}_{1-x}\text{Ge}_x$ alloys, X-ray-absorption fine-structure (XAFS) measurements of strained and relaxed alloys MBE-grown on Si (001) substrates^{28,29} have recently confirmed the dominant (60–71%) Bragg-Pauling character of the composition dependence of the bond length. The strain in crystalline $\text{Si}_{1-x}\text{Ge}_x$ alloys is obviously mainly accommodated by a change of the bond angle rather than bond length.²⁸ In addition, for relaxed single-crystalline $\text{Si}_{1-x}\text{Ge}_x$ alloys, the composition significantly influences the bond length of Si-Ge and Ge-Ge.^{28,29} In contrast to crystals, the bond length and the angles do not depend much on the composition if the $\text{Si}_{1-x}\text{Ge}_x$ alloy is in the amorphous state.^{29,30} Assuming similar behavior of amorphous and liquid phases, a significant change of bond length and angles should occur during track solidification accompanied by an increased probability of incorporating defects into the regrown lattice. This assumption is in good agreement with experimental data of solid-phase epitaxial growth of $\text{Si}_{1-x}\text{Ge}_x$ alloys.^{31–33} In particular, the nonmonotonic compositional dependence of both the activation energy and the pre-exponential factor of the solid-phase crystallization velocity^{31,32} was interpreted by the presence of “microscopic strain” due to differences of the actual bond length and the natural bond length³³ at the interface of the amorphous and crystalline $\text{Si}_{1-x}\text{Ge}_x$ alloy.

The formation of ion tracks will also be affected by other processes such as segregation of the dopant and/or creation of a new phase. It was demonstrated that $\text{Si}_{1-x}\text{Ge}_x$ alloys grown by nonequilibrium methods have ordered regions,^{34,35} where Ge-Ge and Si-Si dimers are preferentially arranged on various planes. During epitaxy, the formation of 2×1 ordered structures can be formed due to segregation of Ge at the Si/Ge interface.³⁵ Similarly, a surface segregation of common dopants in Si and SiGe alloys occurs during epitaxial growth.³⁶ The presence of arsenic on the (001) surface of Si also has the deleterious effect of reducing the regrowth rate.³⁷

Swift heavy ion induced formation of 5–10-nm large GeAs precipitates in the $\text{Si}_{0.5}\text{Ge}_{0.5}$ regions heavily doped with As [Figs. 4(b) and (d)] can probably be used as an

approach for controlled creation of quantum dots (QD's).³⁸ Regular arrays of *equidistant* semiconductor islands of *spherical* shape and *identical* size can be achieved by applying the following two steps: (i) MBE growth of a multilayer system consisting of several-nm thin $\text{Si}_{0.5}\text{Ge}_{0.5}$ layers *super-saturated* by As and alternated by equilibrium layers, (ii) irradiation of the multilayer system with swift heavy ions. Due to the long ion range, even three-dimensional arrays of QD's may be produced. In addition to the number of layers, the density of the precipitates can be controlled by the irradiation fluences up to 10^{11} – 10^{12} cm^{-2} . Their size is determined by the track diameter (typically around 5–10 nm) depending on the ion species and energy loss. The density and size characteristic of such precipitates are optimal for most type of quantum dots.³⁸ Moreover, the nucleation and growth of the precipitates in the sample volume dictates their near *spherical shape* which is advantageous compared to pyramide- or hut-shaped islands usually obtained with the Stranski-Krastanov growth mode.³⁸ In copper oxide glass, nucleation of Cu clusters induced by MeV ion irradiation has recently been reported by Valentin *et al.*³⁹ However, the cluster formation did not occur by room-temperature irradiations but required a post-irradiation thermal annealing process. Although MeV ion irradiation seems to trigger nucleation of nanoclusters,³⁹ any direct correlation with individual tracks is not clear. It should be emphasized that in our case, we observe nanoprecipitates directly created inside the ion tracks.

V. SUMMARY

In conclusion, by using transmission electron microscopy it is demonstrated that 1.3-GeV U ions create discontinuous tracks in single-crystalline $\text{Si}_{1-x}\text{Ge}_x$ alloys. The composition of the $\text{Si}_{1-x}\text{Ge}_x$ alloy and the arsenic doping have an influence on the morphology and atomic structure of the tracks. Strong indications are presented that track formation in semiconductors is linked to the quenching of a melt phase and subsequent imperfect recrystallization.

ACKNOWLEDGMENTS

The authors are grateful to J. Lundsgaard Hansen for MBE growth. The study was supported by NATO CLG Grant No. 976564 and the Danish Strategic Material Research Program.

*Corresponding author. Electronic address: gaiduk@ifa.au.dk

¹N. Bohr, Mat. Fys. Medd. K. Dan. Vidensk. Selsk. **18**, 1 (1948).

²*Proceedings of the Fourth International Symposiums on Swift Heavy Ions in Matter, Berlin, 1998*, edited by S. Klaumunzer and N. Stolterfoht (Nucl. Instrum. Methods Phys. Res. B **146**, 1998).

³M. Toulemonde, C. Dufour, and E. Paumier, Phys. Rev. B **46**, 14 362 (1992).

⁴J. Vetter, R. Scholz, D. Dobrev, and L. Nistor, Nucl. Instrum. Methods Phys. Res. B **141**, 747 (1998).

⁵O. Herre, W. Wesch, E. Wendler, P. I. Gaiduk, F. F. Komarov, S. Klaumunzer, and P. Meier, Phys. Rev. B **58**, 4832 (1998).

⁶P. I. Gaiduk, F. F. Komarov, V. S. Tishkov, W. Wesch, and E. Wendler, Phys. Rev. B **61**, 15 785 (2000).

⁷P. I. Gaiduk, F. F. Komarov, and W. Wesch, Nucl. Instrum. Methods Phys. Res. B **164–165**, 377 (2000).

⁸F. Komarov, P. Gaiduk, and A. Komarov, Vacuum **63**, 657 (2001).

⁹S. A. Karamyan, Nucl. Tracks Radiat. Meas. **18**, 365 (1991).

¹⁰H. Huber, W. Assmann, S. A. Karamian, H. D. Mieskes, H. Nolte, E. Gazis, M. Kokkoris, S. Kossionides, R. Vlastou, R. Grotzschel, A. Mucklich, and W. Prusseit, Nucl. Instrum. Methods Phys. Res. B **146**, 309 (1998).

¹¹M. Levalois, P. Bogdanski, and M. Toulemonde, Nucl. Instrum.

- Methods Phys. Res. B **63**, 14 (1992).
- ¹²P. Marie, M. Levalois, and E. Paumier, J. Appl. Phys. **79**, 7555 (1996).
- ¹³J. Fage-Pedersen, A. Mesli, and A. Nylandsted Larsen, Phys. Rev. B **62**, 10 116 (2000).
- ¹⁴I. V. Antonova, A. V. Dvurechenskii, A. A. Karanovich, A. V. Rybin, S. S. Shaimeev, and H. Klose, Phys. Status Solidi A **147**, K1 (1995).
- ¹⁵B. Canut, N. Bonardi, S. M. M. Ramos, and S. Della-Negra, in Ref. 2, p. 296; A. Dunlop, G. Jaskierowicz, and S. Della-Negra, in Ref. 2, p. 302.
- ¹⁶A. Colder, O. Marty, B. Canut, M. Levalois, P. Marie, X. Portier, S. M. M. Raimos, and M. Toulemonde, Nucl. Instrum. Methods Phys. Res. B **174**, 491 (2001).
- ¹⁷*Properties of Strained and Relaxed Silicon Germanium*, edited by E. Kasper (INSPEC, London, 1995).
- ¹⁸P. I. Gaiduk, A. Nylandsted Larsen, and J. Lundsgaard Hansen, Thin Solid Films **367**, 120 (2000).
- ¹⁹V. S. Tishkov, P. I. Gaiduk, S. Yu. Shiryaev, and A. Nylandsted Larsen, Appl. Phys. Lett. **68**, 655 (1996); A. Nylandsted Larsen, S. Yu. Shiryaev, P. I. Gaiduk, and V. S. Tishkov, Nucl. Instrum. Methods Phys. Res. B **120**, 161 (1996); P. I. Gaiduk, V. S. Tishkov, S. Yu. Shiryaev, and A. Nylandsted Larsen, J. Appl. Phys. **84**, 4185 (1998).
- ²⁰J. F. Ziegler, J. P. Biersack, and U. Littmark, *The Stopping and Ranges of Ions in Solids* (Pergamon, New York, 1985).
- ²¹J. P. Dismukes, R. Ekstrom, E. F. Steigmeier, I. Kudman, and D. S. Beers, J. Appl. Phys. **35**, 2899 (1964).
- ²²L. Csepregi, E. F. Kennedy, J. W. Mayer, and T. W. Sigmon, J. Appl. Phys. **49**, 3906 (1978).
- ²³P. I. Gaiduk, F. F. Komarov, and V. S. Solov'yev, Radiat. Eff. Lett. Sect. **87**, 305 (1986).
- ²⁴M. H. Grabov, G. H. Gilmer, and A. F. Bakker, in *Atomic Scale Calculations in Materials Science*, edited by J. Tersoff, D. Vanderbilt, and V. Vitek (MRS, Pittsburg, 1989), p. 359.
- ²⁵J. A. Yater and M. O. Thompson, Phys. Rev. Lett. **63**, 2088 (1989).
- ²⁶G. D. Ivlev and E. I. Gatskevich, Appl. Surf. Sci. **143**, 265 (1999).
- ²⁷M. J. Aziz and C. W. White, Phys. Rev. Lett. **57**, 2675 (1986).
- ²⁸J. C. Aubry, T. Tyliczszak, A. P. Hitchcock, J. M. Baribeau, and T. E. Jackman, Phys. Rev. B **59**, 12 872 (1999).
- ²⁹M. C. Ridgway, K. M. Yu, C. J. Glover, G. J. Foran, C. Clerc, J. L. Hansen, and A. Nylandsted Larsen, Phys. Rev. B **60**, 10 831 (1999).
- ³⁰S. Minomura, K. Tsuji, M. Wakagi, T. Ishidate, K. Inoue, and M. Shibuya, J. Non-Cryst. Solids **59–60**, 541 (1983).
- ³¹S. Yu. Shiryaev, M. Fyhn, and A. Nylandsted Larsen, Appl. Phys. Lett. **63**, 3476 (1993).
- ³²P. Kringhøj and R. G. Elliman, Phys. Rev. Lett. **73**, 858 (1994).
- ³³P. Kringhøj, R. G. Elliman, M. Fyhn, S. Y. Shiryaev, and A. Nylandsted Larsen, Nucl. Instrum. Methods Phys. Res. B **106**, 346 (1995).
- ³⁴J. Z. Tischler, J. D. Budai, D. E. Jesson, G. Eres, P. Zschack, J.-M. Baribeau, and D. C. Houghton, Phys. Rev. B **51**, 10 947 (1995), and references therein.
- ³⁵N. Ikarashi, A. Oshiyama, A. Sakai, and T. Tatsumi, Phys. Rev. B **51**, 14 786 (1995).
- ³⁶H.-J. Gossmann, in *Delta-Doping of Semiconductors*, edited by E. F. Schubert (Cambridge University Press, Cambridge, England, 1996), p. 161.
- ³⁷W. Ahmed and D. B. Meakin, J. Cryst. Growth **79**, 394 (1986).
- ³⁸D. Bimberg, M. Grundmann, and N. N. Ledentsov, *Quantum Dot Heterostructures* (J. Wiley & Sons Ltd., London, 1999).
- ³⁹E. Valentin, H. Bernas, C. Ricolleau, and F. Creuzer, Phys. Rev. Lett. **86**, 99 (2001).